CCFE
CULHAM CENTRE FOR FUSION ENERGY

UK Atomic Energy Authority

UKAEA-CCFE-PR(18)12

S. E. Sharapov, H. J. C. Oliver, B. N. Breizman,
M. Fitzgerald, L. Garzotti and JET contributors

MHD spectroscopy of tokamaks with pellets via Alfven eigenmodes

MHD spectroscopy of tokamaks with pellets via Alfven eigenmodes

S. E. Sharapov,[1] H. J. C. Oliver,[2, 1] B. N. Breizman,[2] M. Fitzgerald,[1]
L. Garzotti [1] and JET contributors [3]

[1]CCFE, Culham Science Centre, Abingdon, OX14 3DB, UK
[2]Institute for Fusion Studies, University of Texas at Austin, Austin, Texas, USA
[3]See the author list of "Overview of the JET results in support to ITER" by X. Litaudon et al. to be published in Nuclear Fusion Special issue on the 26th FEC (Kyoto, Japan, 17-22 Oct 2016)

This is a preprint of a paper submitted for publication in
Nuclear Fusion

MHD spectroscopy of tokamaks with pellets via Alfvén Eigenmodes

S.E.Sharapov[1], H.J.C.Oliver[2,1], B.N.Breizman[2], M.Fitzgerald[1], L.Garzotti[1] and JET contributors*

EUROfusion Consortium, JET, Culham Science Centre, Abingdon, OX14 3DB, UK
[1]*CCFE, Culham Science Centre, Abingdon, OX14 3DB, UK*
[2]*Institute for Fusion Studies, University of Texas at Austin, Austin, Texas, USA*
**See the author list of "Overview of the JET results in support to ITER" by X. Litaudon et al. to be published in Nuclear Fusion Special issue on the 26th FEC (Kyoto, Japan, 17-22 Oct 2016)*

E-mail contact of main author: Sergei.Sharapov@ukaea.uk

Abstract

Alfvén Eigenmodes (AEs) are routinely seen in present-day tokamaks and stellarators with energetic particles and they represent an attractive form of MHD spectroscopy that provides valuable information on background plasma and on the energetic particles. Possible use of AEs is assessed for MHD spectroscopy of plasma with high-velocity pellet injection employed for fuelling the plasma core. Diagnostics of temporal evolution of the ablated pellets, as well as physics effects determining the diffusion/relaxation of the post pellet profile are of high importance for validating the pellet models and extrapolating them towards ITER. In this paper, JET discharges with ICRH-driven AEs and pellets launched from outboard and inboard tracks are considered. During the pellet injection, an increase in plasma density on a time scale << 50 ms occurs, and several effects on AEs are observed: 1) frequency of the AEs throughout the pellet injection sweeps down by as much as ~30%, 2) the AE amplitudes increase during the AE frequency sweeping, and 3) spectrum of toroidal mode numbers of the AEs broadens significantly after the pellet injection. The effects observed are interpreted in terms of a rise in plasma density and an enhancement of the mode amplitude resulting from the resonance sweeping during the pellet injection.

1 Introduction

In magnetic fusion machines, injection of high speed pellets of frozen hydrogen isotopes (hydrogen, H, deuterium, D, or tritium, T) plays an important role in solving such problems as core fuelling, the isotope mix control, and ELM pacing [1-5]. Also, pellets made of higher-Z atoms (argon, neon) could be used for the disruption mitigation [6, 7]. For each task, the type of the pellet isotope, and the pellet size, velocity, and the repetition rate of the injection are optimised differently. For the fuelling or isotope mix

control, the main consideration is that the usual gas puff to the region around the plasma implies that the gas source at the plasma edge results in rather flat density profiles. A more peaked density profiles could be achieved with fuelling pellets, which have the advantage of producing a higher plasma density in the hotter core plasma region and decreasing the plasma-wall interaction. For sustaining the required plasma density in the core, multiple pellets are injected at an optimised repetition rate. This scenario is limited, however, by the engineering boundaries of the pellet injector, and so the optimisation of the pellet scenarios is usually determined by the engineering or reliability issues rather than physics ones.

For ELM pacing, pellets do not need to penetrate deep into the plasma core, so the pellet velocity could be lower than that required for fuelling. However, the pellet frequency (repetition rate) is important for such scenarios, and the pellet size must be large enough to trigger an ELM. For the pellets made of higher-Z atoms for the disruption mitigation [7], the size of pellets plays a major role as it determines the efficiency of the radiation.

The wide range of the pellet parameters used in various machines for various purposes causes a spread in the characteristic time scales and pellet penetration distances at the pellet ablation. The aim of this paper is to investigate whether diagnosis of the pellet temporal evolution can be addressed by measuring Alfvén Eigenmodes (AEs) that are seen routinely in present-day machines with auxiliary heating and may be naturally abundant in future burning plasmas with large populations of alpha-particles [8]. The AEs are usually numerous, they are easily detectable even at low amplitudes, and their eigenfrequencies are naturally determined by the mass density of the plasma affected by the pellets via

$$\omega_{TAE} \approx \frac{V_A}{2qR_0}, \qquad (1)$$

where the Alfvén velocity $V_A = \frac{B_0}{\sqrt{4\pi\rho}}$ [cm/s] depends on the mass density of plasma,

$$\rho \equiv \sum_i n_i M_i, \qquad (2)$$

which reads $\rho = n_D M_D + n_T M_T$ in the most important case of D-T plasmas, with D density n_D and T density n_T satisfying $n_D + n_T = n_e$, and neglecting plasma impurities and the He ash. During the injection of a pellet at high velocity into the plasma, successive surface layers of the pellet evaporate and are ionised to form a high-density plasmoid along the pellet's path [1-3]. This 3D plasmoid deposited by the pellet is then spread at about the ion sound speed along the magnetic flux surface to provide a

homogeneous density over the surface. Further ∇B drift and diffusion across the magnetic field cause the pellet perturbation to develop into a post-pellet density profile. In the presence of an unstable AE in the area affected by the pellet injection, the dynamics of the mass plasma density could be monitored via the AE spectrum since from (1), (2) one can see that the pellet-induced temporal evolution (increase) of the mass density results in a corresponding change in TAE frequency,

$$\omega_{TAE}(t) \propto 1/\sqrt{\rho(t)}. \quad (3)$$

The use of AEs for MHD spectroscopy, i.e. for understanding properties of magnetically confined plasmas via the measurement of MHD perturbations, is currently widely used for diagnosing temporal evolution of the safety factor in tokamaks [9-11]. It is important to assess whether temporal evolution of the plasma mass density in the case of pellets could be studied with the AEs too. In addition to the study of the density evolution, it is of interest to investigate whether AEs can be used for obtaining information on the fast particle distribution in high density regions caused by the pellets.

2 Experimental setup

The pellet cases analysed in this paper include plasmas run on JET with the centrifugal pellet injector [4, 12] which was able to deliver D pellets with up to $3.8\text{x}10^{21}$ atoms at speed in the range 150-300 m s^{-1}, along one of the three tracks available. The injection trajectories on the poloidal cross-section are shown in Figure 1. Pellets are injected through one of the selected guiding tubes from the top (V), from the inboard (H), and from the outboard (L). Note that all three tracks are not crossing the magnetic axis and so aim at delivering pellets somewhat off-axis as shown in Figure 1; this geometry caused a hollow density profile in many post-pellet JET plasmas.

Line-integrated electron density measurements with high time resolution are provided by an interferometer. The plasma density is integrated along two vertical lines of sight, one of which is close to the magnetic axis (the core line of sight, C), and the other close to the plasma edge at the low field side (E). In all cases considered, the efficiency of the pellet fuelling is determined by the integral of plasma density along the line-of-sight C passing through the magnetic axis at major radius R_0,

$$\hat{n}_e \equiv \int n_e(R = R_0, Z)dZ \ \ [m^{-2}]. \quad (4)$$

In addition, electron density profile could be measured by LIDAR diagnostic [13]. This has a low time resolution, however.

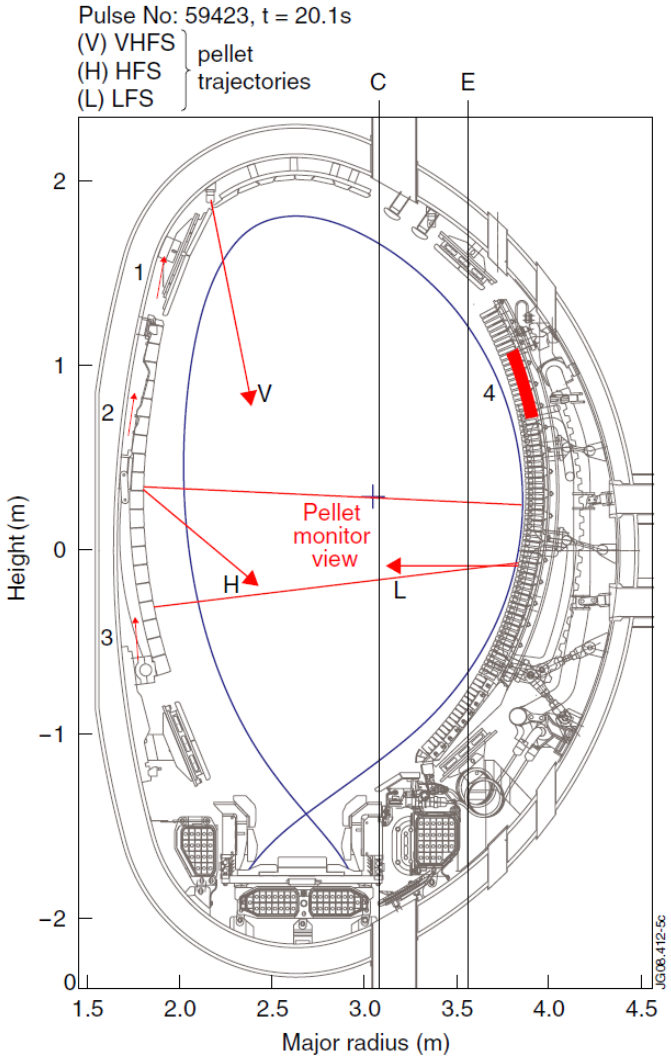

Figure 1. Sketch of the poloidal cross-section of JET with the plasma contour at the last magnetic flux surface (separatrix shown in blue), the pellet injection tracks (H,V,L), the vertical lines of sight of the interferometer passing close to the magnetic axis marked with a cross (plasma core, C) and at the edge (E). Numbers 1 to 3 indicate the position of inboard Mirnov coils, while number 4 indicates the set of outboard toroidally separated Mirnov coils. The red lines without arrows show the pellet monitor view.

Alfvénic perturbations are measured by sets of Mirnov coils just outside the plasma surface. These coils are distributed along the toroidal and poloidal directions and measure perturbed poloidal magnetic field, d $\delta B_p(t)/dt \sim \omega\, \delta B_p(t)$. Due to the rather high frequency of Toroidal AEs and Elliptical AEs, typically in the range of 150 kHz – 450 kHz, the frequency factor in front of the perturbed δB_p is high, so that perturbed magnetic fields could be measured at very low amplitudes down to $\delta B_p/B_0 \leq 10^{-8}$. The toroidal mode numbers n of the AEs excited are deduced from the phase shift of magnetic perturbations measured by outboard coils with the same poloidal position, but separated toroidally.

In all JET cases considered here, AEs are excited by radial gradient of energetic H minority (n_H / n_e ~2-5%) ions obtained in D plasmas with ion cyclotron resonance heating (ICRH) of high power, P_{ICRH} >4 MW. The wave-particle resonances have the form

$$\Omega \equiv \omega - n\,\omega_\varphi - p\,\omega_\theta = 0,\ p=0, \pm 1, \pm 2\ldots \qquad (5)$$

where ω and n are the frequency and toroidal mode number of the AE, ω_φ is toroidal precession frequency, and ω_θ is poloidal bounce-frequency (for trapped ions) or transit frequency (for passing ions). At the nonlinear phase of instability, AEs driven with ICRH in JET have nearly constant saturated amplitudes and eigenfrequencies that follow in time the Alfvén scaling determined by the temporal evolution of the plasma mass density, $\omega \propto B/\rho^{1/2}$ [14].

.

3 TAE evolution in JET discharges with high field side and low field side pellet injection

The efficiency of the pellet fuelling at the plasma core depends on whether the pellets are injected from the high field side or the low field side. The reason for this is that the opposite ∇B-drifts of ions and electrons in the pellet cloud produces a local space charge, and hence a vertical electric field which crosses on the toroidal magnetic field to produce ExB drifts which are directed towards or away from the magnetic axis for high field side and low field side injection geometry, respectively. Here, we investigate in more detail two discharges with AEs, one of which had the pellets injected from the track H, and the other from the track L [14, 15]. Figures 2 and 3 show the background parameters for the discharge with inboard pellet injection (H track) into plasmas with flat current top and $q(0) \approx 1$ (JET pulse #49044 with B_T = 3.25 T, $I_P \leq$ 2.5 MA). The pellets are injected at the velocity of 154 m/s. Figure 2 shows how the set of pellets keep plasma density increased throughout time, with the simultaneous drops in electron temperature after every pellet. The energy content of fast particles essential for excitation of AEs, exhibits a significant drop after first two pellets, and never recovers. Figure 3 shows that after first two pellets, n_e nearly doubles and the n_e-profile becomes hollow. After every of the first four pellets (marked in Figure 4 as A,B,C, and D), the increases in the line-integrated density are $\delta\hat{n}_e \equiv \int \delta n_e(R_0, Z)dZ = 5.44\text{x}10^{19}$ m^{-2} (A), $4.86\text{x}10^{19}$m^{-2} (B), $4.51\text{x}10^{19}$m^{-2} (C), $4.5\text{x}10^{19}$m^{-2} (D). Figure 2 (top) shows that every density increase after the pellet is followed by a decrease in particle confinement that relaxes the density rise down till next pellet is injected.

Figure 4 shows magnetic spectrogram with ICRH-driven AEs observed during the pellet injection. The modes seen before the first pellet A at frequency ~250 kHz are identified as Toroidal AEs (TAEs),

while the weak modes seen at ~450 kHz are Elliptical AEs (EAEs). The activity of AEs becomes very weak (AE amplitudes are small) after ~ 18 s. This is in agreement with the drop in the fast ion energy content from ~ 1.5 MJ to ≤0.5 MJ seen in Figure 2, which is caused by the pellet-induced plasma cooling and plasma density increase, leading to a reduction in the fast ion slowing-down time.

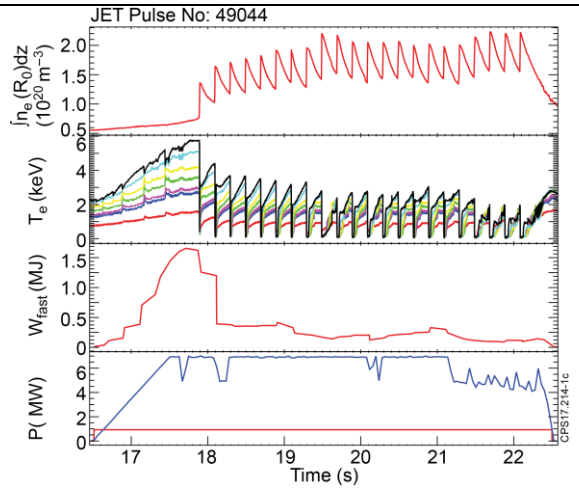

Figure 2. From top to bottom: Line integrated density $\hat{n}_e$ measured with interferometer with the core vertical lines-of-sight (C); Te (keV) measured with multi-channel ECE system at different radii; Fast hydrogen energy content computed with the PION code, and NBI (red) and on-axis hydrogen minority ICRH (blue) power wave forms in JET discharge #49044.

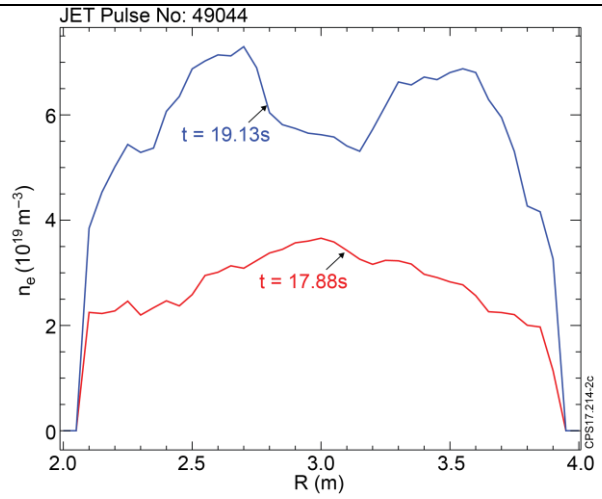

Figure 3. Density profiles in JET discharge #49044 measured before the pellets (red) and after the first two pellets (blue) with LIDAR diagnostic.

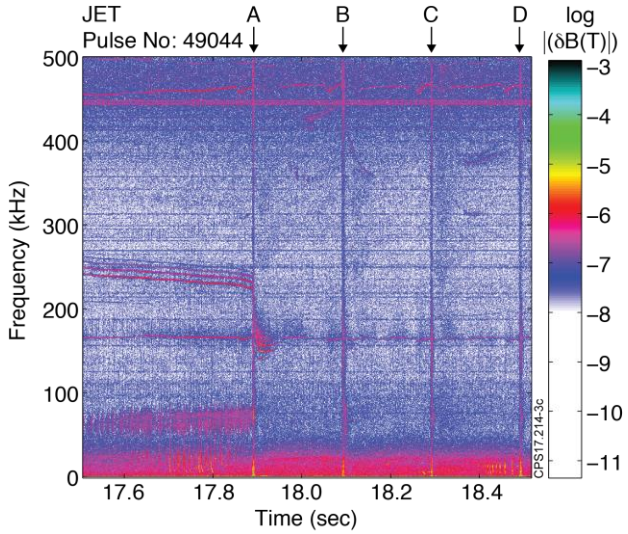

Figure 4. Magnetic spectrogram from the Mirnov coil shows TAEs (~250 kHz), EAEs (~450) and MHD perturbations (vertical lines) caused by the pellets A, B, C, and D (JET pulse #49044).

In order to assess the position of TAEs, to which the pellet A penetrated, the JET equilibrium was reconstructed and modelling with the ICRH code PION and the ideal MHD spectral MISHKA code performed for the TAEs observed. Figure 5 shows the radial profiles of hydrogen minority fast ions computed with the PION code, before the pellets, and just after the second pellet B in JET pulse #49044. Figure 6 shows the computed core-localised TAE with n=7, which is peaked around the maximum gradient of the fast ions shown in Figure 5. Thus we conclude that the pellet penetrated rather deep into the plasma core, $r/a \approx 0.3$, in order to have such a strong immediate effect on TAEs.

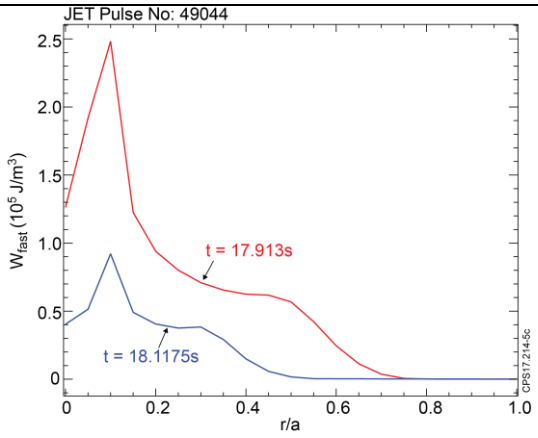

Figure 5 Profiles of fast ion energy density $W_{fast}(r/a)$ from the PION code: just before pellet A (red), and after slowing-down time and pellet B (blue).

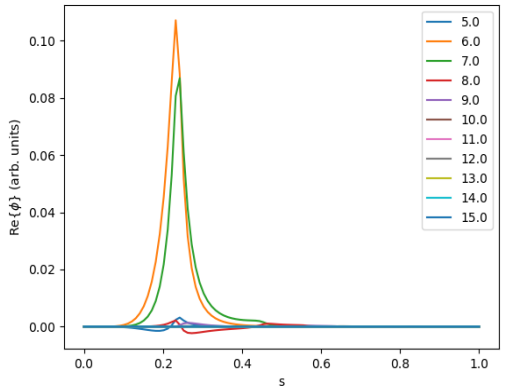

Figure 6 The MISHKA-1 code: Radial structure of the core-localised TAE with n=7 and f_{TAE}=240 kHz computed for JET equilibrium #49044, t=17.88 s. Here, $s = \sqrt{\psi_P / \psi_P(edge)} \approx r/a$ is the normalised radial coordinate, ψ_p is poloidal flux (defined to give zero at the magnetic axis), and ϕ is electrostatic potential of the TAE perturbation.

By zooming the magnetic spectrogram around time of the first pellet A, one can investigate in detail the phenomena seen in TAEs during the pellet injection. Figures 7 and 8 show the details of the amplitude and phase evolutions of TAEs just before, during, and after the pellet A injection.

Inspection of Figures 7, 8 shows that frequencies of TAEs dropped down by ~30% just after the pellet. From the relation $\omega_{TAE}(t) \propto 1/\sqrt{\rho(t)}$ one concludes that such a decrease in TAE frequency should correspond to the plasma density rise of $\approx 80\%$ (at q-profile fixed during the short time of the pellet interaction with the plasma). This significant increase in plasma density is consistent with interferometry measurement in Figure 2 and in line with the LIDAR measurements in Figure 3 made ~ 100 ms later. One concludes that the change in TAE frequency could be used for assessing the mass density increase at the TAE position during a pellet injection.

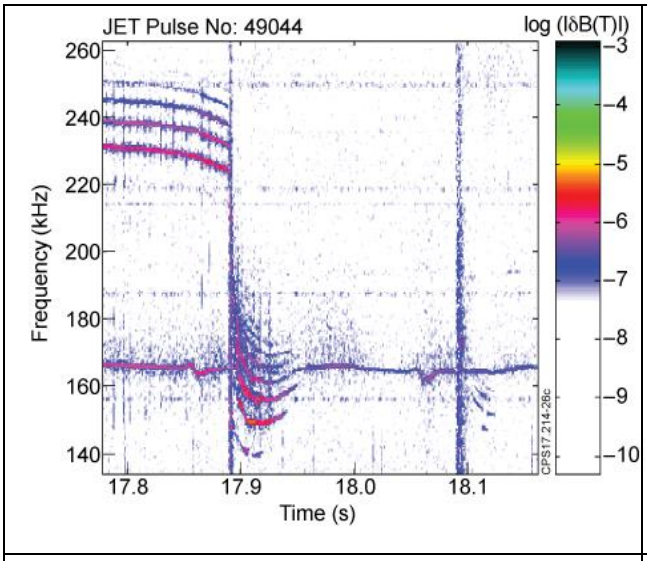

Figure 7 Zoom of the magnetic spectrogram showing amplitudes of the pre-pellet and post-pellet TAEs in JET pulse #49044.

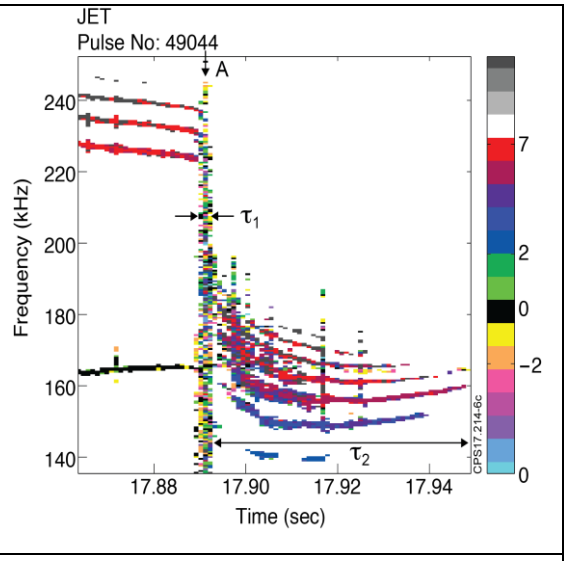

Figure 8 Phase magnetic spectrogram showing pre-pellet TAEs with n=6-9 and post-pellet TAEs with n=3-9. Time of the pellet A injection is marked at the top.

Next we note that the time scale of TAE frequency sweep after the pellet injection is τ_1 ~ 5-8 ms, which is consistent with typical time scale of the pellet ablation [3-5], while the time of post-pellet TAE existence is τ_2 ~ 40 ms consistent with the PION calculations shown in Figure 2. The finite time of TAE observations after the pellet, in accordance with the PION modelling, is caused by the reduction in the fast ion drive at significantly decreased energy content of the fast ions. One concludes then that the AE measurements could also deliver information on the pellet temporal evolution and, to some extent, on the fast ion population at the position of TAE.

In addition, one could see that the pellet injection affected the frequency separation of TAEs, which is mostly caused by Doppler shift due to toroidal rotation of the plasma. In the case of Figures 7,8, we observe a reduction in the toroidal rotation from ~ 8 kHz to ~ 5.6 kHz.

The effects described above could be understood within the existing modelling and be readily employed for the purposes of MHD spectroscopy. There are, however, two more effects visible in Figures 7, 8, which are new and hence require an additional study. First, some post-pellet TAEs were not observed before the pellet injection. Figure 8 shows that a broader spectrum of toroidal mode numbers exists in the post-pellet plasma than in the pre-pellet. Second, Figure 7 shows that amplitudes of TAEs after the pellet are somewhat higher than those before the pellet. Discussion of possible explanation of these effects is presented in the next Section.

Consider now a JET discharge similar to pulse #49044, but with the pellet injected from the low field side. Figure 9 shows the parameters for the discharge with outboard pellet injection (L track) into plasmas with flat current top and $q(0) \approx 1$ (JET pulse #49221 B_T = 3.2 T, $I_P \leq 2.5$ MA), and Figure 10 shows the phase magnetic spectrogram of TAEs with toroidal mode numbers n=2-7 seen at the time of the pellet injection. In this case, the pellets are injected at the velocity of 150 m/s. Again, one could see how the plasma density increases after every pellet, T_e drops, and the energy of fast particle content exhibits a drop down after first pellet. After the pellets A and B, the increases in the line-integrated density are $\delta\hat{n}_e \equiv \int \delta n_e(R_0, Z)dZ = 8.36\text{x}10^{18}$ m^{-2} (A), $3.58\text{x}10^{19}$m^{-2} (B).

Figure 10 shows magnetic spectrogram with ICRH-driven AEs observed during the pellet injection. The modes seen before the first pellet A at frequency ~205 kHz – 230 kHz are TAEs, and frequency of these TAEs sweeps down and up as the pellet cycle goes on.

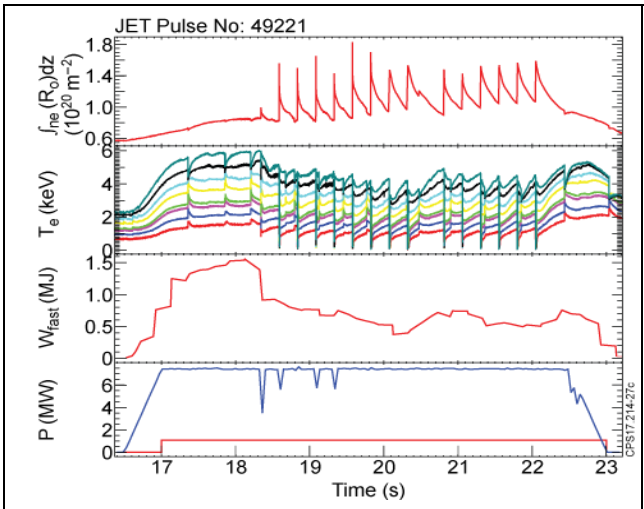

Figure 9 Outboard (L track) pellets in JET pulse #49221 (B_T=3.2 T, I_P^{max}=2.5 MA). From top to bottom: $\int n_e(R_0)dZ$ [m^{-2}] (interferometer); T_e at different R from ECE; fast ion energy content W_{fast} from PION code; ICRH (blue) and NBI (red) power wave-forms.

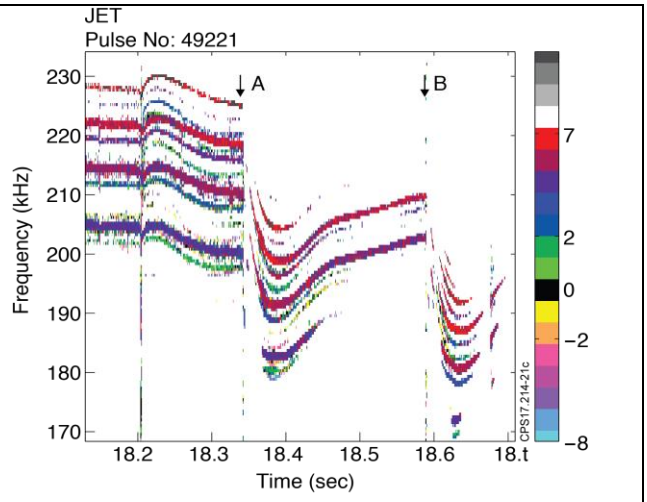

Figure 10 TAEs with n=2-7 in JET #49221. Times of injecting pellets A and B are shown.

From the observations of TAEs, one sees that TAE frequencies drop down by ~ 7.5% only after the pellet A. From the relation $\omega_{TAE}(t) \propto 1/\sqrt{\rho(t)}$ one concludes that such decrease in the frequency corresponds to the plasma mass density rise of ≈ 15% only. This value is much less than that achieved with the inboard pellet launch from H-track. Taking into account that the pellets were nearly similar in their size and velocity in both H-track and L-track cases, one concludes that plasma fuelling with pellets launched from the high field side is much more effective. This is in agreement

with the expected effect of the ∇B drift, and is also confirmed by the interferometer and LIDAR measurements available for these discharges.

Next, the time scale of TAE frequency sweep after the pellet injection is $\tau_1 \sim 15$ ms. This time is much longer than the sweeping rate timescale observed in the case with inboard launch of the pellets considered above. The reduction in the frequency separation of TAEs from ~10 kHz to ~8 kHz is also less significant in the L-track pellet launch than in the H-track launch indicating that the toroidal rotation of plasma is less affected by the pellet. The life-time of TAEs after pellet B is $\tau_2 \sim 100$ ms, which is in agreement with the PION code modelling.

Finally, in the case of the pellet launch from the low field side, the effects of the broadening of the spectrum of toroidal mode numbers of TAEs and TAE amplitude increase are less pronounced than in the case of the high field side pellet launch.

Altogether, the comparison of TAE evolution in plasmas with pellets launched from the high field side and the low field side, shows a more significant density increase in a shorter time, in agreement with the expected effect of ∇B drift on the plasmoids resulting from the pellet ablation [3-5]. This conclusion on the less significant effects of the pellets on plasma density at low field side injection is also in agreement with LIDAR measurements of the plasma density shown in Figure 11. The PION modelling also shows a less significant decrease in fast ion energy content in this case, see Figure 12.

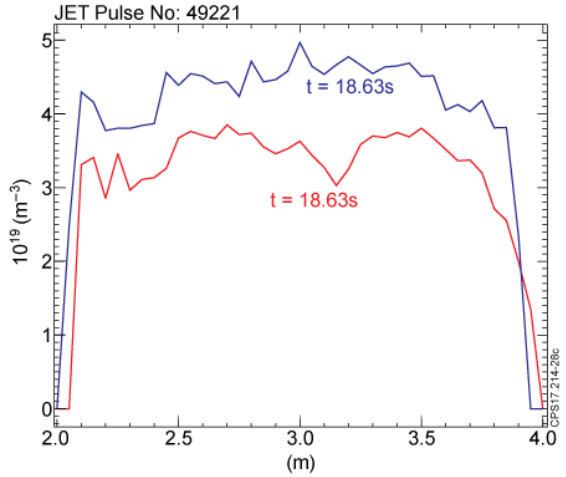

Figure 11 LIDAR: $n_e(R)$ profiles in JET pulse #49221: after pellet A (red), and after pellet B (blue)

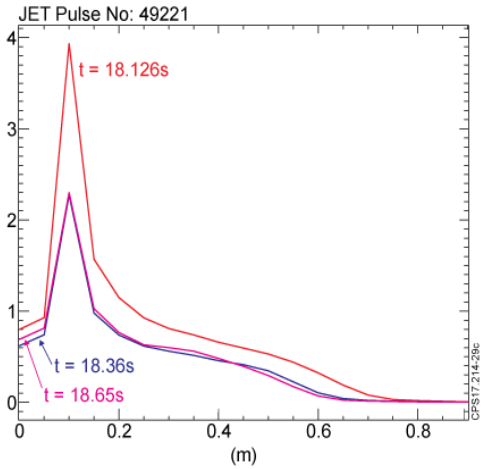

Figure 12 PION: Profiles of fast ion energy density $W_{fast}(r/a)$ before the pellets (red), after pellet A (blue), and after pellet B (pink).

4 Possible enhancement of wave-particle energy exchange due to resonance sweeping

We consider now whether more JET cases exist with a post-pellet TAE spectrum showing more

unstable TAEs (in the number of modes and/or in their amplitudes) than the pre-pellet TAE spectrum, as was seen in the case of JET pulse #49044 above. Figures 13, 14 show another example of such kind. In JET pulse # 49032, the pellet injected at 18.2085 s from the H-track at velocity of ~180 m/s caused a relatively small density increase of $\delta\hat{n}_e = 1.7$ x 10^{19} m^{-2}, but triggered many TAEs with toroidal mode numbers in the range of n = -6,-5…,+2. Note that the negative toroidal mode numbers of TAEs excited indicate that the modes are most likely driven by velocity gradients of the fast ion population (e.g. via bump-on-tail instability).

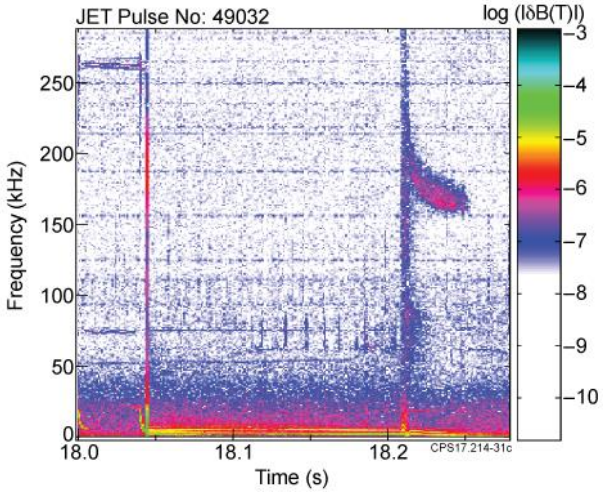

Figure 13 Amplitude magnetic spectrogram showing excitation of post-pellet TAEs at ~18.2 s in the frequency range of ~160-180 kHz in JET pulse #49032.

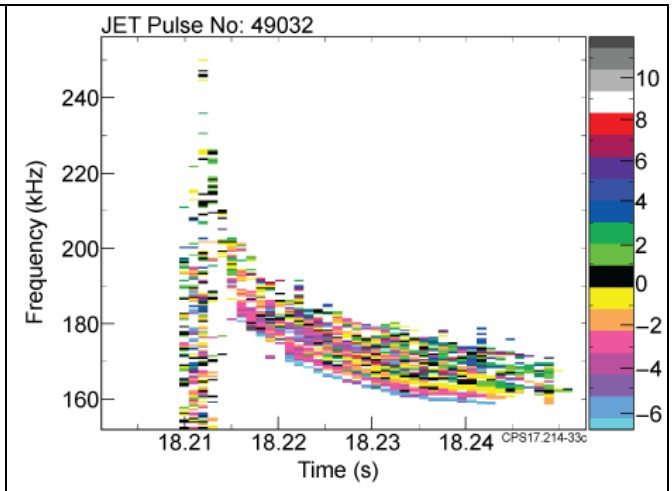

Figure 14 Zoom of Fig.13 showing toroidal mode numbers n= - 6,…, +2 of the post-pellet TAEs in JET #49032.

Another case showing only post-pellet TAEs in the absence of any pre-pellet TAEs is shown in Figures 15, 16. In this JET pulse # 49230 with low ICRH power insufficient to excite TAEs, pellets were injected at time intervals of ~ 27 ms from the H-track at velocity of ~160 m/s. A significant spread was observed in the plasma density increase, e.g. the first two pellets shown in Figure 15 caused $\delta\hat{n}_e = 3.8$ x 10^{18} m^{-2} and 1.34 x 10^{19} m^{-2}. However, every pellet injected was followed by excitation of a TAE, which was stable otherwise in the absence of the pellets, see Figure 16. Due to low mode amplitudes, it was not possible to measure toroidal mode number of these post-pellet TAEs.

The search of effects, which could possibly explain more unstable TAEs in the post-pellet plasmas than in pre-pellet ones (seen in Figures 8, 13, and 16) led to a hypothesis that the resonance sweeping naturally present during pellet injection and decrease in TAE frequency may enhance the wave-particle interaction as discussed in theory [16]. In this theory, the effect of resonance sweeping

is shown to move the mode to the region of a fresh unperturbed distribution function of energetic particles, which provide more free energy to the mode growth than the initial phase space region.

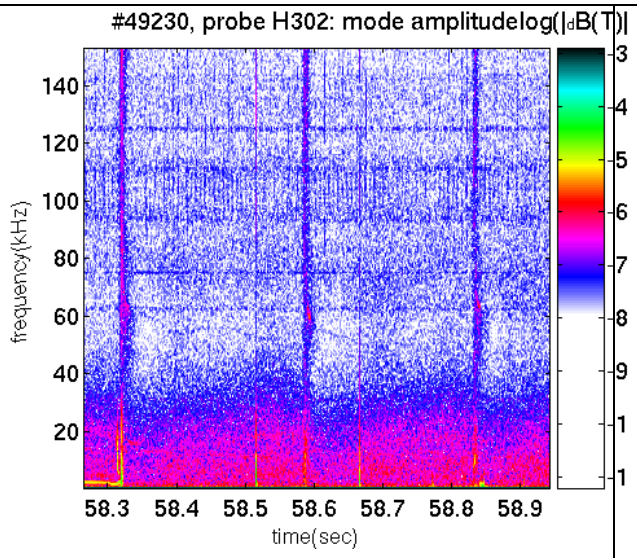

Figure 15 Magnetic spectrogram showing MHD perturbations in JET pulse #49230. Pellets injected are seen as vertical lines.

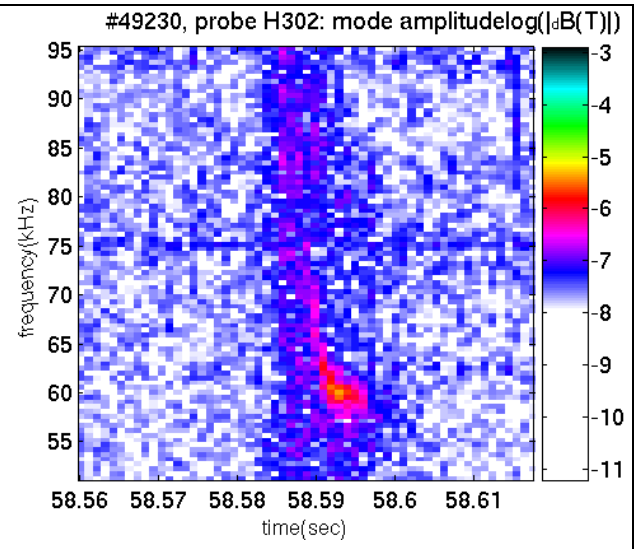

Figure 16 Zoom of Fig.15 showing a post-pellet TAE in JET #49230.

This theory states that i) when the resonance for wave-particle interaction is varied adiabatically, the energy exchange is enhanced and higher amplitude of instability is achieved and ii) this mechanism could even allow excitation of the instability in a system in which background dissipation suppresses linear instability. Both conclusions look compatible with the JET observations but dedicated modelling is yet to be performed to validate the theory. Here, we only perform a direct comparison of the resonance maps showing the phase space regions, in which fast trapped hydrogen ions resonate with a TAE mode (Figures 17, 18). The white colour regions in these Figures correspond to the maximum of the plotted function log (1/Ω), which correspond to the resonance condition (5). These resonance maps have nearly the same structure of the resonances across whole range of the frequencies swept in JET case #49044, from ~235 kHz to ~160 kHz if the trapped fast ions are core-localised, Z < 0.6 m (corresponding to $r/a \leq$ 0.4, which agrees well with the mode and fast ion population localisations shown in Figures 5, 6). Furthermore, the structure of the resonances shows lines at an oblique angle to the energy axis. These resonance maps indicate then that at Z<0.6 m, TAE frequency may sweep down all the way from ~235 kHz to ~160 kHz without losing the wave-particle resonance interaction as ions over a broad energy range, 200 keV < E <800 keV could all resonate with such TAE.

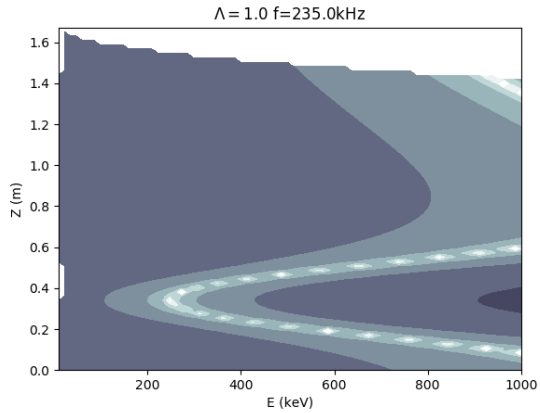

Figure 17 Plot of log (1/Ω) (a.u.) showing the resonance map for pre-pellet TAE with n=7 and ω=235 kHz.

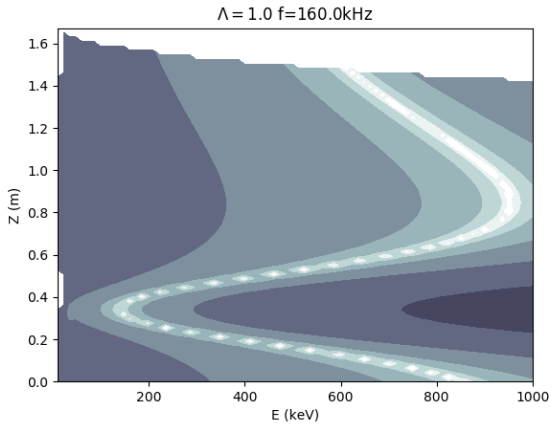

Figure 18 Plot of log (1/Ω) (a.u.) showing the resonance map for post-pellet TAE with n=7 and ω=160 kHz.

5 Dynamics of Ellipticity-induced AEs (EAEs) in JET discharges with pellets

Some JET discharges with ICRH do exhibit higher activity of higher-frequency EAEs than TAEs. This is the case of JET pulse #49220 shown in Figures 19, 20. EAEs may be a good diagnostic tool for MHD spectroscopy too, but usually the area occupied by ICRH-driven EAEs is further from the plasma core than that of TAEs, and so the information on the pellet dynamics obtained from EAEs corresponds to a somewhat different plasma radius.

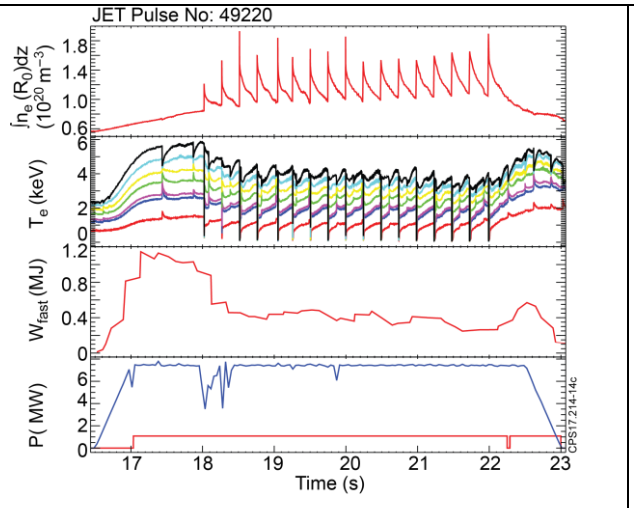

Figure 19 Outboard (L track) pellets injected at 150 m/s in JET pulse #49220 (B_T=3.2 T, I_P^{max}=2.5 MA), from top to bottom: $\int n_e(R_0)dZ$ [m^{-2}] (interferometer); T_e at different R from ECE; Fast ion energy content W_{fast} from PION code; ICRH (blue) and NBI (red) power.

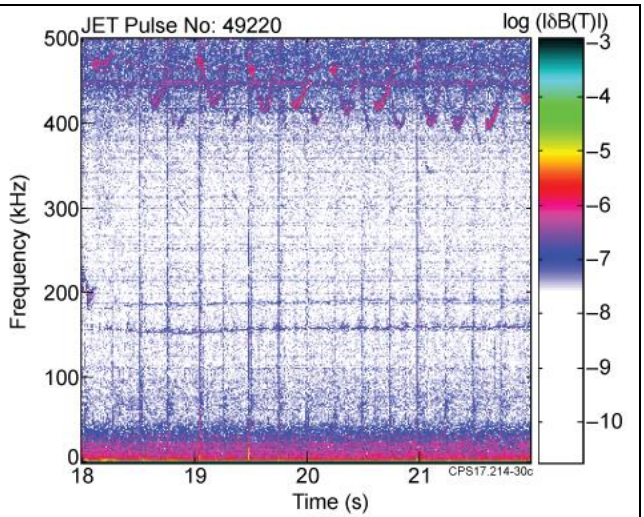

Figure 20 Magnetic spectrogram showing strong EAEs at ~400-500 kHz in JET #49220. TAEs are seen only briefly at the beginning at ~ 200 kHz

Figure 21 shows that EAEs driven by ICRH-accelerated ions, do behave in accordance with the plasma mass density cyclic evolution (increase in density just after the pellet with decrease that follows).

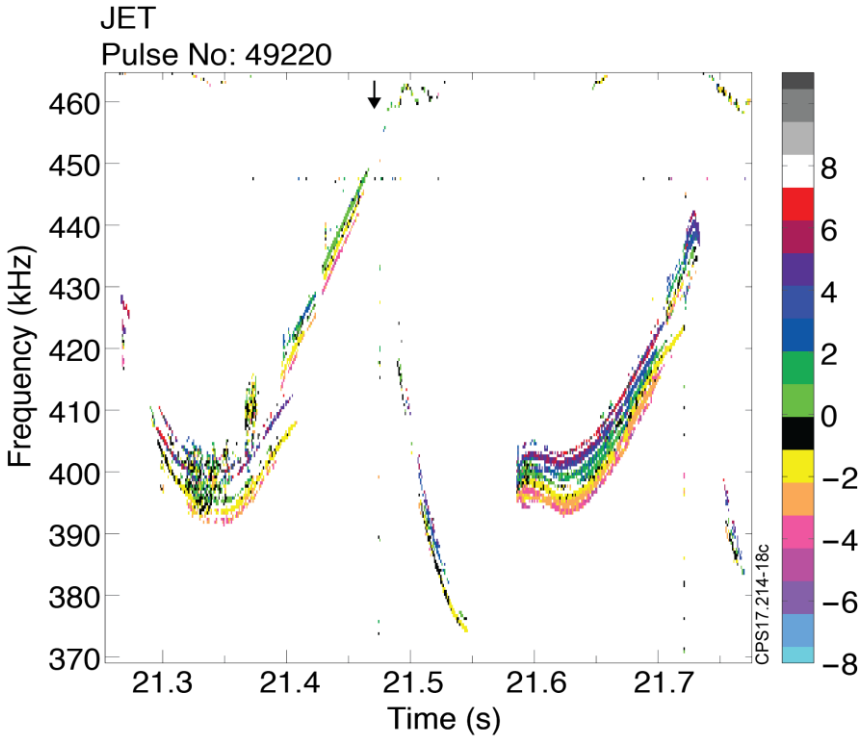

Figure 21 Phase magnetic spectrogram showing colour-coded toroidal mode numbers *n*'s of EAEs excited in JET pulse #49220. Both positive and negative toroidal mode numbers are seen pointing out that the modes are likely to be driven by velocity gradients (since in such cases the drive does not reverse sign with n). The very small frequency separation indicates low Doppler shifts due to the toroidal rotation of plasma close to the edge. The time of the pellet is marked with an arrow on top of the Figure.

If both TAEs and EAEs are seen prior to pellet injection, the frequencies of both modes drop when a pellet is injected into the plasma. The phase space of particles interacting with TAEs and EAEs are separate, suggesting that the frequency changes are caused by the increase in density only, rather than non-linear effects induced by the pellet. The fractional change in the TAE frequencies is more drastic than that of the EAEs. This is consistent with previous observations that EAEs exist further out radially, where the density increase due to the pellet is more moderate compared to the inner core. The decrease of the frequency occurred over a longer period for EAEs compared to TAEs, suggesting the outer core may take longer than the inner core to reach equilibrium after pellet injection. For TAEs, the drop in frequency was immediate upon injection of the pellet. For EAEs, the

decrease was usually immediate, but occasionally a delay of ≈8-20ms was measured before the EAE frequency responded to the pellet. This delay is significantly longer than the pellet transit time, ≈5-6 ms, and the pellet ablation time, ≈5-8 ms. Possible explanations for such time delays have yet to be found.

6 Pellet injection in JET discharges with high power off-axis ICRH and hollow energetic particle profiles

In some JET discharges with very high ICRH power, $P_{ICRH} \leq 10$ MW, massive AE activity was observed in the frequency ranges of TAE, EAE, and NAE (triangularity-induced AEs). The very significant population of fast ions makes such plasmas a good test-bed for testing techniques of MHD spectroscopy, which could be suitable for burning plasmas. Figures 22, 23 show an example of such JET discharge, pulse #49777. In this discharge, ICRH was applied off-axis and hot ion pressure profile was hollow as PION results show in Figure 23.

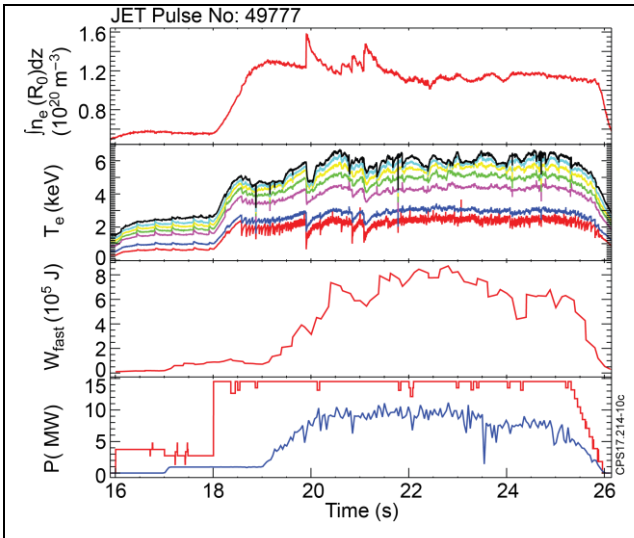

Figure 22 Inboard (H track) pellets in JET pulse #49777 (B_T=2.6 T, I_P^{max}=2 MA): Top to Bottom $\int n_e(R_0)dZ$ [m^{-2}] (interferometer); T_e at different R from ECE; Fast ion energy content W_{fast} from PION code; ICRH (blue) and NBI (red) power.

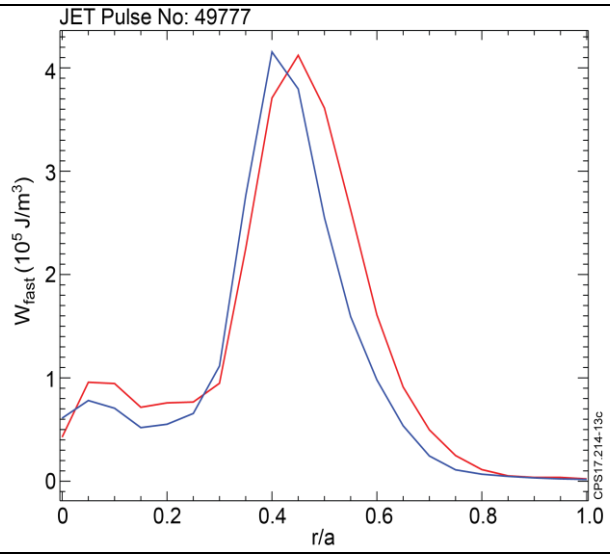

Figure 23 PION: Fast ion energy density profiles at 20.8 s (red), just before pellet C, and after it, at 21.136 s (blue).

Figures 24, 25 show the amplitude and the phase magnetic spectrograms for this discharge. The phase spectrogram shows that a mixture of both positive and negative toroidal mode numbers was observed, with somewhat larger number of modes with n<0. This is expected for the hollow fast ion profile shown in Figure 23.

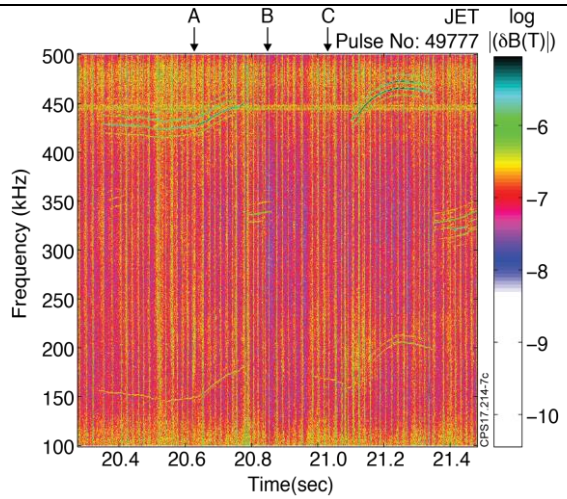

Figure 24 Magnetic spectrogram showing amplitudes of TAEs, EAEs, and, possibly, NAEs in JET #49777. Times of pellet injections A, B, and C are marked at the top of the Figure.

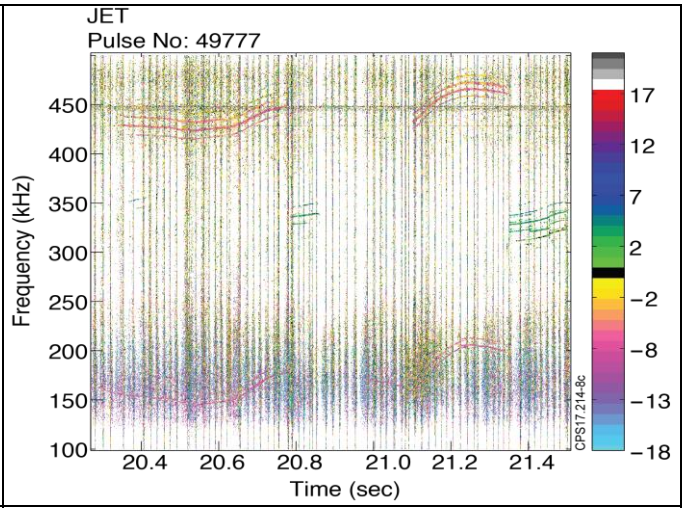

Figure 25 Phase magnetic spectrogram showing toroidal mode numbers of TAEs, EAEs, and NAEs in JET #49777.

7 Summary

In summary, pellets injected into plasmas cause significant changes in AEs, from which MHD spectroscopy could deliver the following information with high time resolution:

i) Mass density increase (information on ion density and isotope mix);

ii) Characteristic times of pellet evolution;

iii) Characteristic times of fast ion slowing down after the pellet;

iv) Evolution of plasma toroidal rotation evolution.

It was found that EAEs could also be used for MHD spectroscopy, but with some additional analysis required for the occasionally observed delays in EAE frequency sweep after the pellet injection. Two new effects associated with pellet injection into plasma with fast ions were observed: transient increase in AE amplitude and excitation of sub-critical post-pellet AEs. An explanation of these effects is likely to be found in the framework of the resonance sweeping theory enhancing the particle-to-wave power transfer.

This work has been carried out within the framework of the EUROfusion Consortium and has received funding from the Euratom research and training programme 2014-2018 under grant agreement No 633053 and from the RCUK Energy Programme [grant number EP/P012450/1]. To obtain further information on the data and models underlying this paper please contact PublicationsManager@ccfe.ac.uk. The views and opinions expressed herein do not necessarily reflect those of the European Commission.

References

[1] Parks P.B. and Turnbull R.J., Phys. of Fluids **21** (1978) 1735;

[2] Macaulay A.K. Nucl. Fusion **34** (1994) 43;

[3] Garzotti L. et al., Nucl. Fusion **46** (2006) 73;

[4] Lang P.T. et al 2007 Nucl. Fusion **47** 754;

[5] Pégourié B. et al., Nucl. Fusion **47** (2007) 44;

[6] Kuteev B.V. et al., Nucl. Fusion **35** (1995) 1167;

[7] Sergeev V.Yu. et al., Plasma Phys. Reports **32** (2006) 363 ;

[8] Sharapov S.E. et al., Fusion Sci, and Tech. **53** (2008) 989;

[9] Goedbloed J.P. et al., Plasma Phys. Control. Fusion **35** (1993) B277 ;

[10] Sharapov S.E. et al., Phys. Lett. A289 127 (2001);

[11] Fasoli A. et al., Plasma Phys. Control. Fusion **44** (2002) B159 ;

[12] Poli F.M. et al., Nucl. Fusion **50** (2010) 025004;

[13] Salzmann H. et al., Rev. Sci. Instruments **59** (1988) 1451 ;

[14] Fasoli A. et al., Phys. of Plasmas **7** (2000) 1816 ;

[15] Testa D. et al., IAEA TCM on Energetic Particles, Gothenburg (2001);

[16] Berk H.L., Breizman B.N., *Enhancement of particle-wave energy exchange by resonance sweeping*, Preprint IFSR #722 (1996).